

# Constraining BSM discrete flavor symmetries with heavy scalar searches at colliders

A. E. Cárcamo Hernández

*Universidad Técnica Federico Santa María and Centro Científico-Tecnológico de Valparaíso, Casilla 110-V, Valparaíso, Chile.*

C. Espinoza

*Cátedras Conahcyt, Departamento de Física Teórica, Instituto de Física, Universidad Nacional Autónoma de México, Apartado Postal 20-364, 01000 CDMX, México.*

J. C. Gómez-Izquierdo

*Centro de Estudios Científicos y Tecnológicos No 16, Instituto Politécnico Nacional, Pachuca: Ciudad del Conocimiento y la Cultura, Carretera Pachuca Actopan km 1+500, San Agustín Tlaxiaca, Hidalgo, México.*

J. Marchant González

*Universidad Técnica Federico Santa María and Centro Científico-Tecnológico de Valparaíso, Casilla 110-V, Valparaíso, Chile.*

M. Mondragón

*Departamento de Física Teórica, Instituto de Física, Universidad Nacional Autónoma de México, Apartado Postal 20-364, 01000 CDMX, México.*

Received 16 May 2023; accepted 18 September 2023

Discrete Flavor Symmetries are often employed in Beyond the Standard Model (BSM) constructions to successfully recreate fermion masses and mixing patterns through several known mechanisms. Obvious constraints on these types of scenarios are the non-observation of Flavour Changing Neutral Currents, which set stringent limits. In this letter, we will discuss the strategy of using the scalar sector phenomenology predicted by such BSM models, and its correlation with the dark matter sector, to further strengthen the constraints by exploiting the large data available from heavy scalar searches in colliders including recent likelihood profiles provided by ATLAS and CMS.

*Keywords:* Multi-Higgs phenomenology; discrete symmetries; dark matter.

DOI: <https://doi.org/10.31349/SuplRevMexFis.4.021126>

## 1. Introduction

The standard model (SM) of elementary particles has reached the status of a paradigm, securing itself a place in the history of fundamental scientific breakthroughs and achievements of humankind. Yet, despite its successes in explaining many phenomena, there are still several questions that it cannot answer. Known issues within the SM are *e.g.* the baryon asymmetry, the muon anomalous magnetic moment, the hierarchy and the strong CP problems, and the existence of dark matter (for a pedagogical review, see *e.g.* [1]). Among the theoretical frameworks with a variety of proposals to address these problems, the addition of discrete symmetries to the SM has some very interesting phenomenological consequences.

Discrete symmetries can be used to predict the masses of fermions in extensions of the SM, collectively referred to as beyond the standard model (BSM) theories. These symmetries can be spontaneously broken, leading to realistic fermion mass hierarchies and mixing patterns such as a quark mixing matrix compatible with the Wolfenstein parametriza-

tion, and a lepton mixing matrix close to the tribimaximal pattern. In some models, the tiny masses of light active neutrinos are produced by an inverse seesaw mechanism mediated by three right-handed Majorana neutrinos. These models successfully accommodate the experimental values of the SM fermion mass and mixing parameters. Constraints on these type of models come mostly from the matter sector where the fermion mass spectra together with the mixing patterns and the strong experimental limits from flavor changing neutral currents represent natural restrictions that limit this kind of theories.

Other interesting BSM models are proposals of extended scalar sectors comprising two or more  $SU(2)$  scalar doublets possibly accompanied by additional scalar singlets or even triplets (a pedagogical review is *e.g.* [2]). These extensions of the SM have been partially motivated by top-down theoretical constructions such as supersymmetric models where a minimum of two scalar doublets is required *e.g.* by holomorphicity of the superpotential and to avoid triangle anomalies. More recently, hints for new resonances at the LHC possibly

of new scalar particles appear to be supported by multiple potential excesses seen at Atlas and CMS, just as (coincidentally?) seen at LEP some years ago, though all these excesses have small global significance. With the tons of data yet to be collected and analyse at the LHC it is very attractive to study the possibility of an extended scalar sector and its phenomenology.

At the time of writing, it is scarce the literature analysing a combination of both of these ideas. To our knowledge, most of previous studies analyse either the matter sector or the scalar one. Here, we briefly report on our efforts wherein we show that it is also possible to constrain discrete flavor symmetries by analysing the scalar sector phenomenology, where *e.g.* limits from experimental scalar searches complement nicely other constraints from the matter or dark matter sectors. For brevity, we shall focus on the scalar sector of the models considered, a more complete and detailed analysis can be found in [3,4].

## 2. $S_4$ Model

The first model that we present here corresponds to an extended three Higgs doublet model (3HDM) where an additional electrically neutral gauge singlet scalar field odd under

a preserved  $Z_2$  discrete symmetry is introduced. Some of the scalars have nontrivial charges with respect to the  $S_4$  discrete symmetry, we have chosen the  $S_4$  family symmetry because it is the smallest non-Abelian discrete symmetry having a singlet, doublet and triplet irreducible representations allowing to naturally accommodate the three fermion families of the SM. The scalar doublets  $\Xi_i$ ,  $i = 1, 2$ , are accommodated in an  $S_4$  doublet while  $\Xi_3$  and the gauge singlet are taken as  $S_4$  singlets.

We address the discussion of the phenomenology of the scalar sector of this model in the low energy regime. As a consequence of the fact that the  $Z_2$  odd scalar  $\phi$  is an  $SU(2)$  singlet the low energy phenomenology of the scalars  $\Xi_i$  is negligibly influenced by the presence of the dark sector. We mainly focus on collider limits for the new scalars predicted by the inclusion of the extra Higgs doublets. We expect deviations of the matter sector relative to the SM to be of negligible influence in the phenomenology of the scalar sector at present accelerator searches. Thus, we consider [2] a matter sector where the third generation of quarks and charged leptons couples only to  $\Xi_3$ , and we neglect the masses of the first and second family of fermions. After the spontaneous breaking of the  $S_4$  discrete symmetry, the low energy scalar potential of the model under consideration takes the form:

$$\begin{aligned}
V = & -\mu_1^2 \left( \Xi_1^\dagger \Xi_1 \right) - \mu_2^2 \left( \Xi_2^\dagger \Xi_2 \right) - \mu_3^2 \left( \Xi_3^\dagger \Xi_3 \right) + \lambda_1 \left( \Xi_1^\dagger \Xi_1 + \Xi_2^\dagger \Xi_2 \right)^2 + \lambda_2 \left( \Xi_2^\dagger \Xi_1 - \Xi_1^\dagger \Xi_2 \right)^2 \\
& + \lambda_3 \left[ \left( \Xi_1^\dagger \Xi_2 + \Xi_2^\dagger \Xi_1 \right)^2 + \left( \Xi_1^\dagger \Xi_1 - \Xi_2^\dagger \Xi_2 \right)^2 \right] \\
& + \lambda_4 \left[ \left( \Xi_1^\dagger \Xi_2 + \Xi_2^\dagger \Xi_1 \right) \left( \Xi_1^\dagger \Xi_3 + \Xi_3^\dagger \Xi_1 \right) + \left( \Xi_1^\dagger \Xi_1 - \Xi_2^\dagger \Xi_2 \right) \left( \Xi_2^\dagger \Xi_3 + \Xi_3^\dagger \Xi_2 \right) \right] \\
& + \lambda_5 \left( \Xi_3^\dagger \Xi_3 \right) \left( \Xi_1^\dagger \Xi_1 + \Xi_2^\dagger \Xi_2 \right) + \lambda_6 \left[ \left( \Xi_3^\dagger \Xi_1 \right) \left( \Xi_1^\dagger \Xi_3 \right) + \left( \Xi_3^\dagger \Xi_2 \right) \left( \Xi_2^\dagger \Xi_3 \right) \right] \\
& + \lambda_7 \left[ \left( \Xi_3^\dagger \Xi_1 \right)^2 + \left( \Xi_3^\dagger \Xi_2 \right)^2 + \left( \Xi_3 \Xi_1^\dagger \right)^2 + \left( \Xi_3 \Xi_2^\dagger \right)^2 \right] + \lambda_8 \left( \Xi_3^\dagger \Xi_3 \right)^2 .
\end{aligned} \tag{1}$$

Stability conditions for the potential are calculated numerically employing the public tool EVADE [3,4], which features the minimization of the scalar potential through polynomial homotopy continuation [5] and an estimation of the decay rate of a false vacuum [6,7]. From the expression for the potential we obtain the square mass matrices for the physical CP-even scalars  $h$ ,  $H_3$ ,  $H$ , the pseudo-scalars  $A$ ,  $A_2$  and the charged scalars  $H^\pm$  and  $H_2^\pm$ , where we define  $h$  as the SM-like Higgs. We assume the vev alignment  $v_1 = v_2$  and next we discuss analytical approximations for the CP-even scalars masses, let us denote the mass matrix by the expression:

$$\mathbf{M}_{CP\text{-even}}^2 = \begin{pmatrix} a & d & f \\ d & b & e \\ f & e & c \end{pmatrix} . \tag{2}$$

Explicit expressions for these matrix elements as a function of the model parameters can be found in the appendix of [7]. Except for cases where one or several entries of this matrix are zero or cases where there are degenerate eigenvalues, we can approximate the masses of these physical scalars by the expressions [8]:

$$\begin{aligned}
m_h^2 &= \frac{1}{3} (a + b + c - 2\sqrt{x_1} \cos[\Xi_s/3]) , \\
m_H^2 &= \frac{1}{3} (a + b + c + 2\sqrt{x_1} \cos[(\Xi_s - \pi)/3]) , \\
m_{H_3}^2 &= \frac{1}{3} (a + b + c + 2\sqrt{x_1} \cos[(\Xi_s + \pi)/3]) ,
\end{aligned} \tag{3}$$

where

$$x_1 = a^2 + b^2 + c^2 - ab - ac - bc + 3(d^2 + f^2 + e^2), \quad (4)$$

and

$$\Xi_s = \begin{cases} \arctan\left(\frac{\sqrt{4x_1^3 - x_2^2}}{x_2}\right) & , \quad x_2 > 0, \\ \pi/2 & , \quad x_2 = 0, \\ \arctan\left(\frac{\sqrt{4x_1^3 - x_2^2}}{x_2}\right) + \pi & , \quad x_2 < 0, \end{cases} \quad (5)$$

with

$$x_2 = -(2a - b - c)(2b - a - c)(2c - a - b) + 9[(2c - a - b)d^2 + (2b - a - c)f^2 + (2a - b - c)e^2] - 54def. \quad (6)$$

From the above definitions, we notice that  $\Xi_s \in [-\pi/2, 3\pi/2]$ , thus,  $m_H$  is always greater than  $m_h$ , but  $m_{H_3}$  can be smaller than  $m_h$ . However, we will explore in detail a region of parameter space where  $m_{H_3}$  is greater than  $m_h$  which is then the lightest of the three, and this is the reason for choosing it as the SM-like Higgs.

In general, Eqs. (3) are not suitable for eliminating some quartic couplings or other parameters in favor of the square masses. This represents a disadvantage at the numerical level since we have to enforce the constraint that the mass of  $h$  has to be very close to 125.5 GeV. This results in very inefficient scans of parameter space because a large proportion of the test points in parameter space don't yield such a value for the mass of the Higgs-like scalar. In an effort to trade generality for the possibility to perform a thorough exploration of a region of parameter space compatible with the value of the Higgs mass, we enforce the equation:

$$x_2 = 0, \quad (7)$$

by suitable choosing one of the quartic couplings ( $\lambda_5$ ) so that Eq. (7) is satisfied. This can always be done since this equation is a quadratic in  $\lambda_5$ , and we choose this coupling since it does not appear in the expressions of the masses of the pseudo scalars nor the charged scalars. Henceforth, we will be presenting a numerical analysis of the parameter slice  $\Xi_s = \pi/2$ . In this hyper-region of parameter space, the equations for the masses (3) not only take a simple form but also allow eliminating two more quartic couplings ( $\lambda_1$  and  $\lambda_8$ ) in favor of  $m_{H_3}$  and  $m_h$ . In this way we gain control over the values of these masses, and from the relation:

$$\Delta \equiv \sqrt{x_1/3} = m_H^2 - m_{H_3}^2 = m_{H_3}^2 - m_h^2, \quad (8)$$

which follows from the simplified equations of the masses, we see that in the explored slice of parameter space we have the hierarchy  $m_H^2 > m_{H_3}^2 > m_h^2$  and that these squared masses are separated by the same mass gap  $\Delta$ . We shall refer to this slice as the symmetric gap region. Having control over the value of these masses allows us to perform a scan of parameter space in which we choose the mass of  $h$  to be in a small interval (given by the current experimental error bars) around 125.5 GeV. We then vary the mass of  $H_3$  in the interval  $m_h < m_{H_3} < 1$  TeV, while that of  $H$  is determined from the value of  $\Delta$  and  $m_{H_3}^2$ .

---

For the numerical computations, we implement the model in 9, 10, 11, 12 from which we generate corresponding model files for some of the other tools using the SARAH-SPheno framework [13–15]. When testing a given point of parameter space, for positivity and stability of the scalar potential we use EVADE, while exclusion limits from scalar searches at Tevatron, LEP and the LHC are implemented with the aid of HiggsBounds [16]. We impose hard cuts discarding points not complying with these constraints. For points not filtered by the previous hard cuts we calculate numerically the model predicted observables that are used to construct a composite likelihood function. We calculate the couplings and decay branching ratios of the 125 GeV SM Higgs-like and the rest of the scalars with the help of the SARAH generated SPheno code. In particular, we use the decay probabilities of the heavy scalars and pseudo scalars into pairs of  $\tau^+\tau^-$  leptons in order to compare these predictions with the recent search of the ATLAS collaboration involving these type of resonances decaying into  $\tau$ -lepton pairs [17]. This specific ATLAS search was motivated because such decay modes can be enhanced in multi-Higgs models relative to the SM predictions. A higher cross section for Higgs boson production in association with  $b$  quarks ( $bbH$ ) can also occur in such scenarios, making this production channel competitive with the main gluon fusion production ( $ggF$ ). We calculate  $bbH$  and  $ggF$  cross section productions for all neutral scalars using SUSHi [18, 19].

In what follows, we make extensive use of likelihood-based statistical tests commonly used in high energy physics for the discovery of new phenomena and for construction of confidence intervals on model parameters. A detail exposition of these methods can be found in [20]. We use the above predictions of the model to construct the composite likelihood function:

$$\log \mathcal{L}_{\text{scalar}} = \log \mathcal{L}_{\text{Higgs}} + \log \mathcal{L}_{\text{ATLAS}}, \quad (9)$$

using public numerical tools. We obtain the likelihood  $\log \mathcal{L}_{\text{Higgs}}$  that measures how well the couplings of the SM Higgs-like  $h$  resemble that of the already discovered SM Higgs using HiggsSignals [20]. For the likelihood  $\log \mathcal{L}_{\text{ATLAS}}$  which implements the public data from the AT-

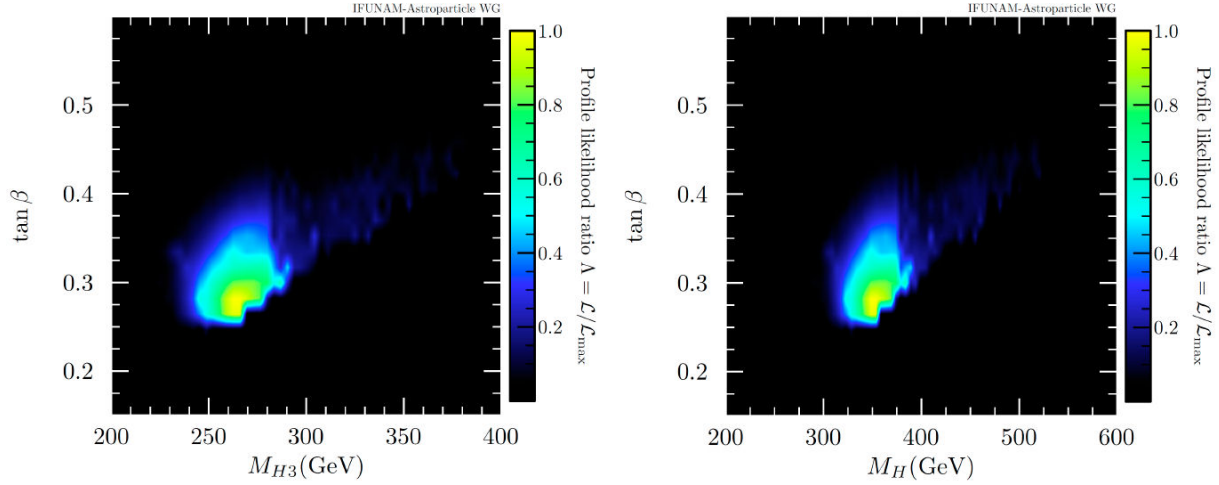


FIGURE 1. Composite likelihood as a function of the CP-even scalar masses and  $\tan \beta$ .

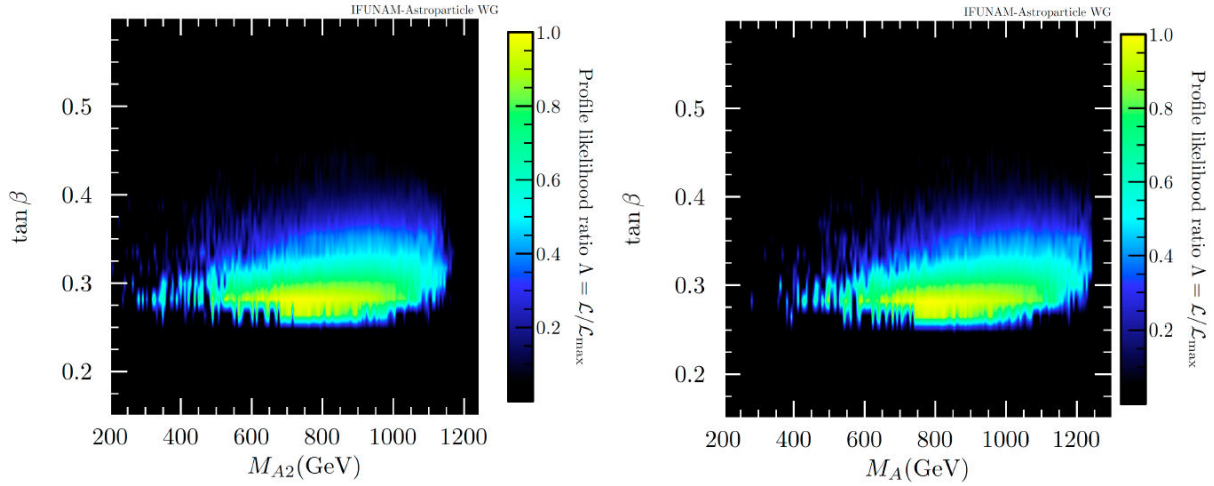


FIGURE 2. Composite likelihood as a function of the CP-odd scalar masses (first column), the charged scalars (second column), and  $\tan \beta$ .

LAS search mentioned before, we make use of the capabilities of `HiggsBounds` [16,21]. Finally, we perform the scan of the parameter space and construct the likelihood profiles using `Diver` [22,23] (in standalone mode).

Figure 1 shows the obtained profile likelihoods with respect to Eq. (9) for the case of the masses of the CP-even scalars  $H$  and  $H_3$  and its correlation with the value of  $\tan \beta$ . We note that the phenomenological analysis results in the model's consistency with observations only for small values of  $\tan \beta$ . This parameter appears to be constrained at a confidence level (CL) of 95% to take values in between  $\sim 0.25$  and  $\sim 0.45$  at the preferred values of the masses at the best fit point (BFP). The masses of  $H_3$  and  $H$  most favored lie in  $\sim 263$  GeV and  $\sim 350$  GeV respectively. The analysis allows to constrain these masses in respective intervals of  $\sim 50$  GeV and  $\sim 75$  GeV with a CL of 68%, though the constraining interval worsens considerably at the 95% of CL.

The corresponding likelihood profiles for the pseudo-scalars and the charged scalars is shown in Fig. 2. The constraining interval over the value of  $\tan \beta$  is consistent with

the previous figure, however in these cases the values of the masses are limited very poorly.

We now describe the dark sector of the model. We couple the  $Z_2$  odd scalar field to the active scalars in a minimalistic way and consistent with their  $S_4$  assignments. The scalar potential is taken as the sum of the active scalars potential shown before with the respective one containing the dark scalar:

$$V_{\text{DM}} = V - \mu_\phi \phi^2 + \lambda_\phi \phi^4 + \lambda_9 \phi^2 \left( \Xi_1^\dagger \Xi_1 + \Xi_2^\dagger \Xi_2 \right) + \lambda_{10} \phi^2 \left( \Xi_3^\dagger \Xi_3 \right), \quad (10)$$

where for simplicity we have assumed  $\phi$  to be real, and  $V$  is given by Eq. (1). We keep checking the stability of each potential numerically and maintain the hard cuts described in the previous section. While the model has fermion DM candidates [1], we deem much more interesting the case of a scalar lightest ( $Z_2$ ) odd particle (LOP), where thanks to the couplings of the dark scalar to the active ones it is possible

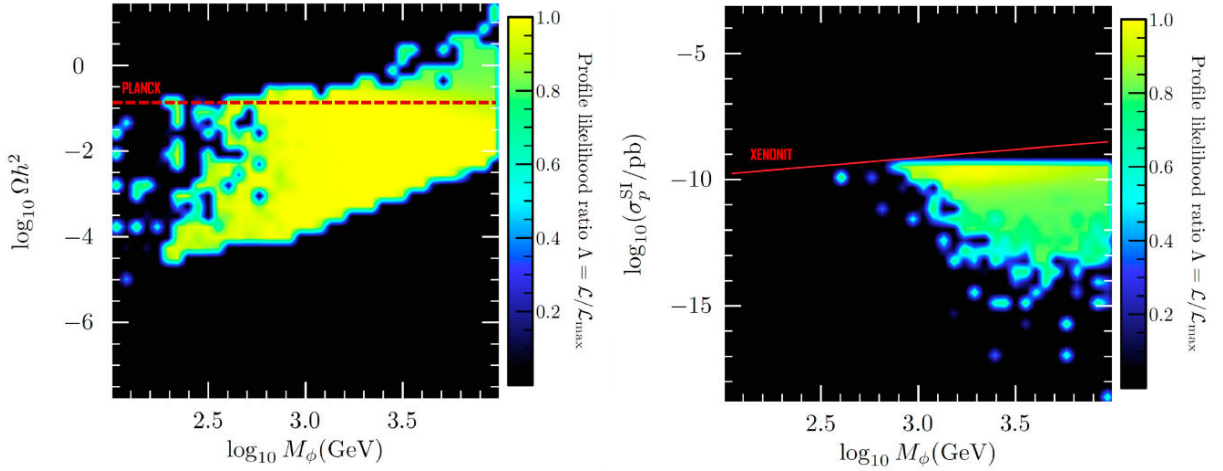


FIGURE 3. Left panel: Partial composite likelihood (not including the relic density likelihood) as a function of the DM candidate mass and its relic density. The Planck measured value [24] is marked by the dashed horizontal line. Right panel: Composite likelihood as a function of the DM candidate mass and SI DM-proton cross section for the case that the candidate represents 100% of the DM in the Universe. Also shown is the 90% CL upper limit from the  $1t \times 1yr$  XENON1T experiment.

to have tree level scattering amplitudes between a scalar LOP and quarks, allowing the phenomenological analysis of direct detection (DD) of such candidate. Thus,  $\phi$  is our DM candidate, with this rationale, we construct a log-likelihood function involving the observables in the (visible) scalar sector previously discussed, and the DD and relic abundance observables:

$$\log \mathcal{L} = \log \mathcal{L}_{\text{scalar}} + \log \mathcal{L}_{\text{DD}} + \log \mathcal{L}_{\Omega h^2}. \quad (11)$$

For the numerical calculation of the relic density as well as the DM-nucleon scattering cross sections we use the capabilities of `Micromegas` [25–28]. We construct  $\mathcal{L}_{\Omega h^2}$  as a basic Gaussian likelihood with respect to the PLANCK measured value, while the likelihood  $\mathcal{L}_{\text{DD}}$  involves publicly available data from the direct detection XENON1T experiment [29]. We use the numerical tool `DDCalc` to compute the Poisson likelihood given by

$$\mathcal{L}_{\text{DD}} = \frac{(b+s)^o \exp\{-(b+s)\}}{o!}, \quad (12)$$

where  $o$  is the number of observed events in the detector and  $b$  is the expected background count. From the model's predicted DM-nucleon scattering cross sections as input, `DDCalc` computes the number of expected signal events  $s$  for given DM local halo and velocity distribution models (we take the tool's default ones, for specific details on the implementation such as simulation of the detector efficiencies and acceptance rates, possible binning etc. see [30, 31]).

It is instructive to analyze the slice of parameter space involving the value of the relic abundance, taking into account the partial likelihood without the factor involving the relic density likelihood. To this end, we define:

$$\log \mathcal{L}_{\text{S+DD}} = \log \mathcal{L}_{\text{scalar}} + \log \mathcal{L}_{\text{DD}}. \quad (13)$$

With respect to this partial likelihood, we show in the left panel of Fig. 3 the likelihood profiles of the relic abundance

prediction as a function of the DM candidate mass. (Note that the corresponding plot with the full log-likelihood is just a slim horizontal bright band around the Planck measured value).

More than two thirds of the explored parameter space results in an underabundant prediction for the DM candidate. The analysis yields a pattern where DM masses as low as 1 TeV and lighter predict abundances (with discernible likelihood ratio value) from close to the Planck measure, all the way down to around  $10^{-4}$ . It is possible to discern a tendency that as the DM mass increases the lowest value attained for the relic density raises (sort of linearly) towards the Planck limit. Above a certain mass no points in parameter space can be found that yield a likelihood ratio greater than 0.1. This upper mass bound appears to be a little bit above 10 TeV.

In the right panel of Fig. 3, we present the profile likelihood with respect to the full log-likelihood (11) for the model normalized to the value of  $\mathcal{L}$  at the point of maximum likelihood (the brightest region) assuming the DM candidate constitutes 100% of the DM in the Universe. The plot shows the dependence of the likelihood on the DM mass and the DM-proton spin independent (SI) cross section. We also depict the 90% CL upper limit on the SI cross section from the XENON1T ( $1t \times yr$ ) experiment [29]. We can see from this figure that the DM candidate is strongly constrained by the analysis. There is only a very small region of parameter space with a likelihood ratio above  $\sim 0.8$  in the neighborhood of  $M_\phi \sim 3.98$  TeV. Due to the constraints from the XENON1T observations, the allowed region lies below the respective exclusion curve.

Next, we present a similar analysis for a BSM model but now with non-Abelian  $Q_4$  discrete symmetry. The discrete symmetry denominated by  $D_N$  is the symmetry of a regular polygon of  $N$  sides, and occurs in nature *e.g.* in poly-atomic molecules. The discrete non-Abelian group  $Q_4$ , also known

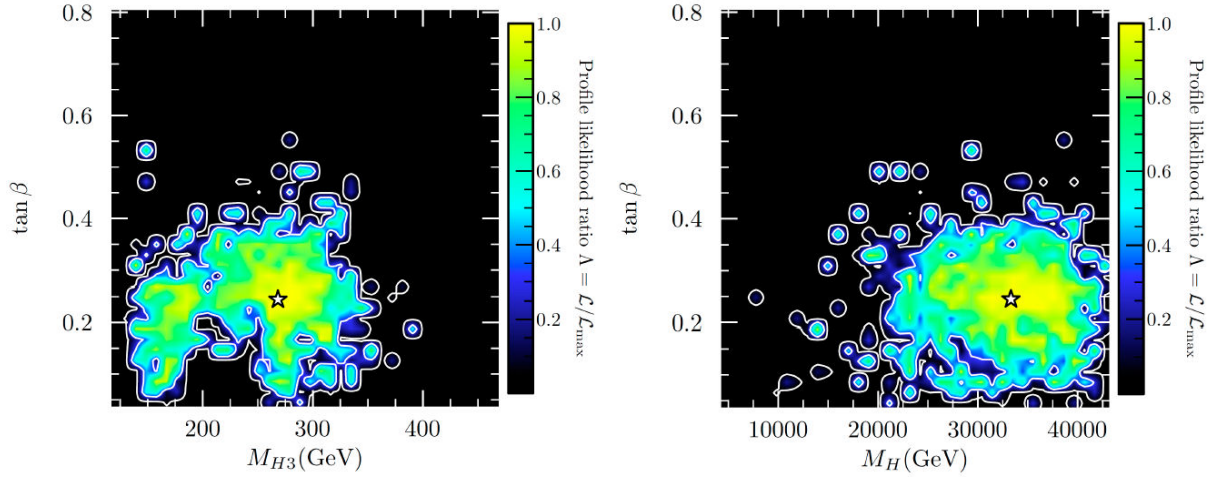


FIGURE 4. Composite likelihoods as functions of the scalar masses and  $\tan\beta$ . Contours of 68% and 95% of CL are drawn and the best fit point is marked with a star.

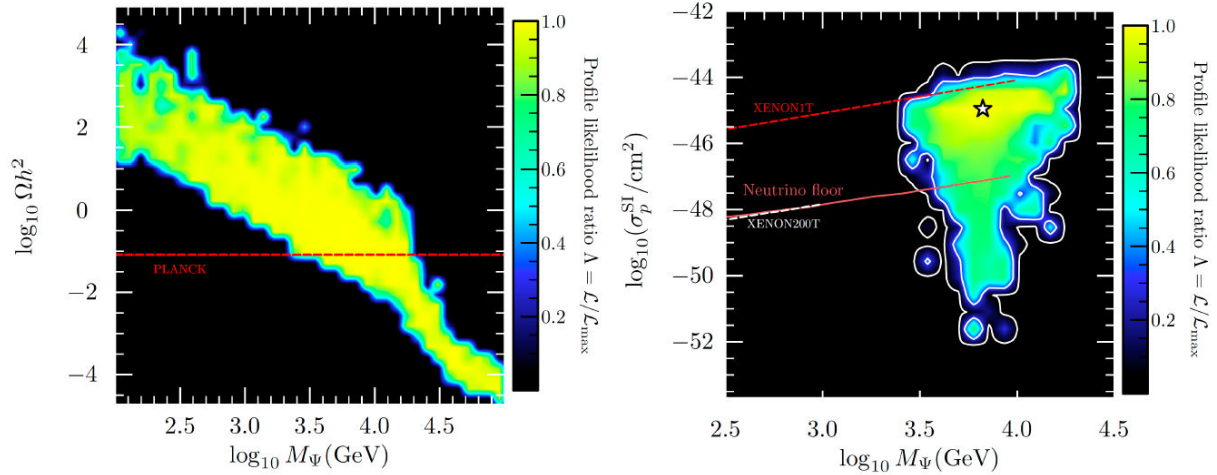


FIGURE 5. Left panel: Composite likelihood (not including the relic density likelihood) as a function of the DM candidate mass and its relic density. The Planck measured value is marked by the dashed horizontal line. Right panel: Composite likelihood as a function of the DM candidate mass and SI DM-proton cross section for the case that the candidate represents 100% of the DM in the Universe. Contours of 68% and 95% of CL are drawn, and also shown are the 90% CL upper limit from the  $1t \times 1yr$  XENON1T experiment, the multi-ton projection to  $200t \times 1yr$  and the neutrino floor. The best fit point is marked with a star.

as the binary dihedral group, can be seen as the group cover of  $D_4$ , and has pseudo-real representations which is advantageous for chiral theories. In this model, we propose a scalar sector with two Higgs doublets  $\Xi_1, \Xi_2$ , and one real scalar singlet  $\varphi$  that mixes with the CP-even scalar. The scalar singlet is further coupled to a right handed heavy neutrino  $\Psi$  which is the DM candidate. We proceed to briefly describe the scalar and DM sectors phenomenology, for full details see [1].

Due to the mixing of the singlet with the real parts of the neutral scalars, we have three CP-even physical scalars, one of which corresponds to a SM Higgs-like particle  $h$ , we take the other two scalars, denoted  $H_3$  and  $H$  as heavier. For the numerical analysis of this model we follow the strategy outlined previously, but we limit ourselves to include the information from the measured values of the relic density  $\Omega h_{\text{Planck}}^2$

and Higgs mass  $m_h$  as basic Gaussian likelihoods  $\mathcal{L}_\Omega$  and  $\mathcal{L}_{m_h}$  respectively. We also include a likelihood function  $\mathcal{L}_{DD}$  based on results from the XENON1T Direct Detection Experiment, we then maximize over the model's parameter space the composite log-likelihood:

$$\log \mathcal{L} = \log \mathcal{L}_{DD} + \log \mathcal{L}_\Omega + \log \mathcal{L}_{m_h}. \quad (14)$$

In Fig. 4, we present the low energy scalar mass spectra of the model, the regions of parameter space that better match high values of the composite log-likelihood are shown as bright zones, and the best fit point (BFP) is marked with a star. From these plots, we thus find that the scalar  $H$  is markedly heavier than  $H_3$  which is around twice as heavy as the SM-like Higgs  $h$ .

In Fig. 5, we present the likelihood profile as a function of the mass of the DM candidate and its relic density (but

not including the likelihood from the relic density, the corresponding plot with the full log-likelihood is just a slim horizontal bright band around the Planck measured value). We infer from this figure that DM candidate masses below  $\sim 2.5$  TeV, though they can be compatible with *e.g.* direct detection limits, they would be overproduced at the freeze out epoch. We observed also that, assuming the DM candidate comprises 100% of the dark matter of the universe, its mass can only be around  $\sim 2.5$  and  $\sim 20$  TeV.

For this model, the DM candidate  $\Psi$  couples to fermions thanks to the mixing between the scalars through a coupling  $y_\Omega \bar{\Psi}\Psi\varphi$ . For simplicity, we will assume the DM Yukawa coupling  $y_\Omega$  to be real. We now present a likelihood analysis involving publicly available data from the direct detection XENON1T experiment [29]. In the right panel of Fig. 5, we present the profile likelihood normalized to the value of  $\mathcal{L}$  at the best fit point (signaled by a star) assuming the DM candidate constitutes 100% of the DM in the Universe. The plot shows the dependence of the likelihood on the DM mass and the DM-proton spin independent (SI) cross section; contours of 68% and 95% of confidence level (CL) are drawn. We also depict the 90% CL upper limit on the SI cross section from the XENON1T ( $1t \times \text{yr}$ ) experiment [29], alongside with the multi-ton-scale time projection to  $200t \times \text{yr}$  of reference [32] and an estimation of the neutrino floor [33]. We note that almost all the region consistent with the constraints including the BFP lies below the zone currently excluded by the XENON1T experiment. However, the figure also makes it evident that the multi-ton projection to  $200t \times 1\text{yr}$  will be capable of probing zones well below the BFP of the model.

### 3. Conclusions

We have presented analysis of the scalar and DM sectors of a couple of BSM models featuring discrete symmetries. In

the analysis of the scalar sector of the  $S_4$  model we made a thorough examination of a specific slice of parameter space characterized by a symmetric gap between the square masses of the CP-even scalars. We compared the predictions of the model with observations from recent searches of ATLAS involving the production of scalar resonances and their decay to  $\tau$ -lepton pairs. Our results allow constraining effectively only the masses of the CP-even scalars and the value of the ratio of their vacuum expectation values, the latter can attain only very small values. In the  $S_4$  model dark sector, by means of a composite likelihood function involving the information from the scalar sector, DD and DM abundance constraints, we were able to identify mass ranges of the DM candidates consistent with the measured DM abundance, as well as the ranges of values of DM-proton scattering cross section consistent with results from the XENON1T experiment. We found that the singlet DM candidate can be strongly constrained by current experimental observations. We performed a similar analysis for a  $Q_4$  model with a fermion DM candidate.

The consistency of our models with the constraints arising from collider searches for heavy scalars, stability of the scalar potentials, the dark matter relic density and current and future direct detection experiments sets stringent limits on the parameter space of the models. In particular, we have shown that the analysis of the scalar sector characteristics and phenomenology gives rise to constraints on models with discrete symmetries that are complementary to the usual constraints from the matter sector such as *e.g.* FCNC.

### Acknowledgements

C.E. acknowledges the support of Conahcyt (México) Cátedra no. 341. This research is partially supported by DGAPA PAPIIT IN109321.

- 
1. A. E. C. Hernández *et al.*, Fermion masses and mixings, dark matter, leptogenesis and  $g - 2$  muon anomaly in an extended 2HDM with inverse seesaw, *Eur. Phys. J. Plus* **137** (2022) 1224, <https://doi.org/10.1140/epjp/s13360-022-03432-w>.
  2. A. E. Cárcamo Hernández *et al.*, Predictive extended 3HDM with  $S_4$  family symmetry (2022), <https://doi.org/10.48550/arXiv.2212.12000>.
  3. W. G. Hollik, G. Weiglein, and J. Wittbrodt, Impact of Vacuum Stability Constraints on the Phenomenology of Supersymmetric Models, *JHEP* **2019** (2019) 109, [https://doi.org/10.1007/JHEP03\(2019\)109](https://doi.org/10.1007/JHEP03(2019)109).
  4. P. M. Ferreira *et al.*, Vacuum Instabilities in the N2HDM, *JHEP* **2019** (2019) 6, [https://doi.org/10.1007/JHEP09\(2019\)006](https://doi.org/10.1007/JHEP09(2019)006).
  5. M. Maniatis and D. Mehta, Minimizing Higgs Potentials via Numerical Polynomial Homotopy Continuation, *Eur. Phys. J. Plus* **127** (2012) 91, <https://doi.org/10.1140/epjp/i2012-12091-1>.
  6. S. Coleman, The Fate of the False Vacuum. I. Semiclassical Theory, *Phys. Rev. D* **15** (1977) 2929, <https://doi.org/10.1103/PhysRevD.15.2929>.
  7. C. G. Callan, and S. Coleman, The Fate of the False Vacuum. II. First Quantum Corrections, *Phys. Rev. D* **16** (1977) 1762, <https://doi.org/10.1103/PhysRevD.16.1762>.
  8. C.-A. Deledalle *et al.*, Closed-form expressions of the eigen decomposition of  $2 \times 2$  and  $3 \times 3$  Hermitian matrices, Research report, Université de Lyon (2017), <https://hal.archives-ouvertes.fr/hal-01501221>.
  9. F. Staub, SARAH 4: A tool for (not only SUSY) model builders, *Comput. Phys. Commun.* **185** (2014) 1773, <https://doi.org/10.1016/j.cpc.2014.02.018>.
  10. F. Staub, From Superpotential to Model Files for FeynArts and CalcHep/CompHep, *Comput. Phys. Commun.*

- 181** (2010) 1077, <https://doi.org/10.1016/j.cpc.2010.01.011>.
11. F. Staub, Automatic Calculation of supersymmetric Renormalization Group Equations and Self Energies, *Comput. Phys. Commun.* **182** (2011) 808, <https://doi.org/10.1016/j.cpc.2010.11.030>.
  12. F. Staub, SARAH 3.2: Dirac Gauginos, UFO output, and more, *Comput. Phys. Commun.* **184** (2013) 1792, <https://doi.org/10.1016/j.cpc.2013.02.019>.
  13. F. Staub, Exploring new models in all detail with SARAH, *Adv. High Energy Phys.* **2015** (2015) 840780, <https://doi.org/10.1155/2015/840780>.
  14. W. Porod, SPheno, a program for calculating supersymmetric spectra, SUSY particle decays and SUSY particle production at  $e^+e^-$  colliders, *Comput. Phys. Commun.* **153** (2003) 275, [https://doi.org/10.1016/S0010-4655\(03\)00222-4](https://doi.org/10.1016/S0010-4655(03)00222-4).
  15. W. Porod and F. Staub, SPheno 3.1: Extensions including flavour, CP-phases and models beyond the MSSM, *Comput. Phys. Commun.* **183** (2012) 2458, <https://doi.org/10.1016/j.cpc.2012.05.021>.
  16. P. Bechtle *et al.*, HiggsBounds-5: Testing Higgs Sectors in the LHC 13 TeV Era, *Eur. Phys. J. C* **80** (2020) 1211, <https://doi.org/10.1140/epjc/s10052-020-08557-9>.
  17. G. Aad *et al.*, Search for heavy Higgs bosons decaying into two tau leptons with the ATLAS detector using pp collisions at  $\sqrt{s} = 13$  TeV, *Phys. Rev. Lett.* **125** (2020) 051801, <https://doi.org/10.1103/PhysRevLett.125.051801>.
  18. R. V. Harlander, S. Liebler, and H. Mantler, SusHi: A program for the calculation of Higgs production in gluon fusion and bottom-quark annihilation in the Standard Model and the MSSM, *Comput. Phys. Commun.* **184** (2013) 1605, <https://doi.org/10.1016/j.cpc.2013.02.006>.
  19. R. V. Harlander, S. Liebler, and H. Mantler, SusHi Bento: Beyond NNLO and the heavy-top limit, *Comput. Phys. Commun.* **212** (2017) 239, <https://doi.org/10.1016/j.cpc.2016.10.015>.
  20. P. Bechtle *et al.*, HiggsSignals-2: Probing new physics with precision Higgs measurements in the LHC 13 TeV era, *Eur. Phys. J. C* **81** (2021) 145, <https://doi.org/10.1140/epjc/s10052-021-08942-y>.
  21. P. Bechtle *et al.*, Applying Exclusion Likelihoods from LHC Searches to Extended Higgs Sectors, *Eur. Phys. J. C* **75** (2015) 421, <https://doi.org/10.1140/epjc/s10052-015-3650-z>.
  22. G. D. Martinez *et al.*, Comparison of statistical sampling methods with ScannerBit, the GAMBIT scanning module, *Eur. Phys. J. C* **77** (2017) 761, <https://doi.org/10.1140/epjc/s10052-017-5274-y>.
  23. P. Scott, Pippi - painless parsing, post-processing and plotting of posterior and likelihood samples, *Eur. Phys. J. Plus* **127** (2012) 138, <https://doi.org/10.1140/epjp/i2012-12138-3>.
  24. N. Aghanim *et al.*, Planck 2018 results. VI. Cosmological parameters, *Astron. Astrophys.* **641** (2020) A6, <https://doi.org/10.1051/0004-6361/201833910>.
  25. G. Bélanger *et al.*, micrOMEGAs\_3: A program for calculating dark matter observables, *Comput. Phys. Commun.* **185** (2014) 960, <https://doi.org/10.1016/j.cpc.2013.10.016>.
  26. G. Bélanger *et al.*, micrOMEGAs4.1: two dark matter candidates, *Comput. Phys. Commun.* **192** (2015) 322, <https://doi.org/10.1016/j.cpc.2015.03.003>.
  27. D. Barducci *et al.*, Collider limits on new physics within micrOMEGAs\_4.3, *Comput. Phys. Commun.* **222** (2018) 327, <https://doi.org/10.1016/j.cpc.2017.08.028>.
  28. G. Bélanger *et al.*, micrOMEGAs5.0: Freeze-in, *Comput. Phys. Commun.* **231** (2018) 173, <https://doi.org/10.1016/j.cpc.2018.04.027>.
  29. E. Aprile *et al.*, Dark Matter Search Results from a One Ton-Year Exposure of XENON1T, *Phys. Rev. Lett.* **121** (2018) 111302, <https://doi.org/10.1103/PhysRevLett.121.111302>.
  30. T. Bringmann *et al.*, DarkBit: A GAMBIT module for computing dark matter observables and likelihoods, *Eur. Phys. J. C* **77** (2017) 831, <https://doi.org/10.1140/epjc/s10052-017-5155-4>.
  31. P. Athron *et al.*, Global analyses of Higgs portal singlet dark matter models using GAMBIT, *Eur. Phys. J. C* **79** (2019) 38, <https://doi.org/10.1140/epjc/s10052-018-6513-6>.
  32. M. Schumann *et al.*, Dark matter sensitivity of multi-ton liquid xenon detectors, *JCAP* **10** (2015) 016, <https://doi.org/10.1088/1475-7516/2015/10/016>.
  33. J. Billard, E. Figueroa-Feliciano, and L. Strigari, Implication of neutrino backgrounds on the reach of next generation dark matter direct detection experiments, *Phys. Rev. D* **89** (2014) 023524, <https://doi.org/10.1103/PhysRevD.89.023524>.